Published in final edited form as:
Biomaterials. 2010 December ; 31(34): 8953–8963. doi:10.1016/j.biomaterials.2010.08.017.

Helicoidal multi-lamellar features of RGD-functionalized silk biomaterials for corneal tissue engineering

Eun Seok Gil[1], **Biman B. Mandal**[1], **Sang-Hyug Park**[1], **Jeffrey K. Marchant**[2], **Fiorenzo G. Omenetto**[1], and **David L. Kaplan**[1,2,*]

[1] Department of Biomedical Engineering, Tufts University, 4 Colby St. Medford, Massachusetts 02155 USA

[2] Sackler School of Biomedical Science, Tufts University, 4 Colby St. Medford, Massachusetts 02155 USA

Abstract

RGD-coupled silk protein-biomaterial lamellar systems were prepared and studied with human cornea fibroblasts (hCFs) to match functional requirements. A strategy for corneal tissue engineering was pursued to replicate the structural hierarchy of human corneal stroma within thin stacks of lamellae-like tissues, in this case constructed from scaffolds constructed with RGD-coupled, patterned, porous, mechanically robust and transparent silk films. The influence of RGD-coupling on the orientation, proliferation, ECM organization, and gene expression of hCFs was assessed. RGD surface modification enhanced cell attachment, proliferation, alignment and expression of both collagens (type I and V) and proteoglycans (decorin and biglycan). Confocal and histological images of the lamellar systems revealed that the bio-functionalized silk human cornea 3D constructs exhibited integrated corneal stroma tissue with helicoidal multi-lamellar alignment of collagen-rich and proteoglycan-rich extracellular matrix, with transparency of the construct. This biomimetic approach to replicate corneal stromal tissue structural hierarchy and architecture demonstrates a useful strategy for engineering human cornea. Further, this approach can be exploited for other tissue systems due to the pervasive nature of such helicoids in most human tissues.

1. Introduction

The human cornea is an avascular tissue comprised of five distinguished layers and at least 3 different cell types with orientation, including the outermost epithelium, the central stroma, and the innermost endothelium [1–3]. The World Health Organization estimates that corneal damage causes significant vision impairment and blindness, second only to cataracts. Allograft cornea transplantation is the most commonly performed option for corneal tissue replacement in the United States, with over 30,000 to 40,000 performed annually [4]. However, the supply of donor corneal tissue worldwide falls well short of the demand. Moreover, corneal grafts can stimulate host immune responses resulting in tissue rejection, or they can transfer diseases from unhealthy donor organs. These complications are compounded by the growing use of corrective eye surgery which renders these corneas unsuitable for grafting, further reducing the

*Corresponding author: Department of Biomedical Engineering, School of Engineering, Tufts University, 4 Colby St, Medford, MA 02155, USA., Tel.: +1 617627 3251, Fax: +1 6176273231, david.kaplan@tufts.edu, (D.L. Kaplan).

availability of acceptable allogenic supplies [5]. Therefore, new options for corneal equivalent biomaterials are needed for the development of clinical devices for corneal replacements.

Successful corneal tissue engineering requires appropriate scaffolds where the cells can proliferate, organize native extracellular matrix, and recapitulate native corneal structure and functions. The corneal stromal layer makes up approximately 90% of the overall cornea thickness and consists of orthogonally aligned collagen fibril layers termed lamellae [6]. Approximately 200 to 250 lamellae extend from limbus to limbus and are stacked with angular offsets. The corneal stroma is populated by keratocytes (what is this question?) which are responsible for the production of heterotypic type I/V collagen fibrils that exhibit uniform diameter and spacing [7,8]. Transparency requires strict limitations on matrix composition and organization and these properties are maintained by the cell layers. The interweaving of collagen bundles between neighboring lamellae provides important structural foundation for shear (sliding) resistance and transfer of tensile loads between lamellae. These highly organized collagen lamellae provide mechanical support and light diffraction properties appropriate for transparency [9]. These structural features present significant design challenges in biomaterial devices as potential replacement options.

Recent interest in engineering cornea equivalents have generated a number of biomaterials for corneal tissue engineering, including collagen hydrogels [10,11], aligned collagen fibrils [2], collagen films [12], and other synthetic polymer systems [13,14]. These approaches to biomaterial designs for corneal tissue engineering can be classified in three categories: engineering the whole cornea, corneal stroma, and epithelium. Efforts to mimic the three layered structure of the cornea (epithelium, stroma, and endothelium) have been reported [15,16]. However, the reconstruction of corneal stroma is challenging due to the complexity of the structural hierarchy, the requirements for mechanical strength and the need to maintain optical transparency. Therefore, engineering corneal stroma has been investigated by developing functional corneal stroma features [17–21]. Engineered epithelium tissue sheets have been clinically evaluated using autologous oral mucosal epithelium [22]. Also, direct *in vivo* implantation of corneal equivalent biomaterials without cells has been investigated to study the integration of implanted biomaterial with native corneal tissue [23,24]. In all cases, none of these studies has provided a solution to the need for replacement human corneas, either due to rejection, material performance limitations or the early stage of the research to date.

Silk fibroin has been utilized in biomaterials for tissue engineering and regenerative medicine due to its biocompatibility [25,26], material stability and mechanical robustness [27,28], and controllable degradability [29,30]. Silk films support cell attachment and proliferation on a comparable scale to tissue-culture plastic [29,31–34]. In addition, silk film surfaces can be modified with nano/micro size patterns, which can direct cells and the orientation of their ECM [33–35]. The transparency of silk films has also recently been demonstrated over the full range of optical wavelengths [36,37]. Therefore, transparent silk film cornea biomaterials may be engineered by providing contact guidance to produce helicoidally oriented multi-lamellar architectures that replicate native corneal stroma features, while also providing a mechanically robust system with controlled but slow biodegradability to support native tissue regeneration.

Many studies have shown that the addition of cell-attachment peptides to various substrates enhances cell adhesion and/or migration [38–42]. With respect to corneal cells, RGD (from fibronectin) and YIGSR (from laminin B1) have been used to promote corneal fibroblast and corneal epithelial cell adhesion, respectively, and type VI collagen has also been shown to promote corneal fibroblast adhesion in and RDG-independent fashion [43]. Our own studies have shown that RGD coupled to silk increases osteoblast-like cell adhesion and expression of both alkaline phosphatase and osteocalcin [26,44,45].

We previously demonstrated the possibility of silk protein-biomaterial lamellar systems coupled with human cornea fibroblasts for corneal stroma engineering [33]. Optically transparent patterned silk films (2 μm thick) were studied to demonstrate feasibility (32), and the influence of different surface patterns on human corneal fibroblast responses were also explored [46]. Although these studies revealed that rabbit or human corneal fibroblasts on patterned silk films replicated anisotropic single lamellar forms of corneal stroma, the multi-stacked corneal stroma constructs revealed random cell and ECM organization. One explanation of this poor cell and ECM alignment in the silk lamellar constructs was the lack of contact guidance of the patterned silk films by the apical contact of cells in the construct. In scaffolding biomaterials, cell spreading is attributed to the interaction of both the apical and basal cellular surfaces with the surrounding matrix; thus similar cell interactions may be taking place within the assembled silk layers. Consequently, there remains a formidable challenge to replicate native corneal stroma forms in silk cornea biomaterials because of the importance of the aligned lamellar architecture in the corneal stroma as described above. The ability to recapitulate this complex structural hierarchy while controlling cell responses would provide a path forward in human corneal replacements.

Given that helicoidally oriented ECM lamellar structure in engineered corneal constructs is crucial to replicate native corneal stroma features and functions, the present study was focused on the replication of angle-ply multi-lamellar ECM organization in transparent silk human cornea biomaterials. Toward this goal, RGD coupling to silk films and their subsequent stacking into 3D constructs was studied to verify the effect of the RGD-coupling on the response of human corneal fibroblasts, to address adequate replication of biological cornea pheonotype, form, and function.

2. Materials and Methods

2.1. Preparation of silk solution

Silk solution was generated from *Bombyx mori* (*B. mori*) silkworm cocoons according to the procedures described in our previous studies [29,47]. Cocoons of *B. mori* silkworm silk were supplied by Tajima Shoji Co (Yokohama, Japan). Briefly, the cocoons were degummed in a boiled 0.02-M Na_2CO_3 (Sigma-Aldrich, St Louis, MO) solution for 30 min. The fibroin extract was then rinsed three times in Milli-Q water, dissolved in a 9.3-M LiBr solution yielding a 20% (w/v) solution, and subsequently dialyzed (MWCO 3,500) against distilled water for 2 days to obtain silk fibroin aqueous solution (ca. 8 wt/vol %).

2.2. Preparation of polydimethylsiloxane (PDMS) substrates

Patterned PDMS (GE Plastics, Pittsfield, MA) substrates were prepared by casting on a reflective diffraction grating as used in previous study (Edmund Optics, Inc., Barrington, NJ). The PDMS substrates were punched into round disks with 14 mm diameters. The PDMS substrates were washed in a 70% ethanol and then thoroughly rinsed in DI water before casting silk solutions on the substrates to generate the patterned films.

2.3. Preparation of silk films

For film preparation, a 100 μL of 1% silk solution was cast on the prepared PDMS substrates with 14 mm in diameter to generate films with a thickness of around 2 μm [48]. The as-cast silk films were water-annealed [29] in a water-filled desiccator at 24 mm Hg vacuum for 5 h. The silk films were immersed in a water bath and removed from the PDMS substrates, and then placed into 24-well plates with the grooved surface facing up. The films were sterilized with 70% EtOH, dried, and washed three times in PBS (pH 7.4). The wells were then filled with 0.5 mL media overnight before cell seeding.

2.4. Preparation of patterned/porous silk films

A mixture of 1% silk fibroin and 0.05% polyethylene oxide (PEO, MW = 900,000; Sigma–Aldrich) solution was prepared to induce pore formation within the silk film matrix. One hundred μL of solution was cast on flat PDMS or patterned PDMS substrates to produce 2 μm film thicknesses. Post-casting, silk films were water-annealed and then placed into a water bath for 3 days to leach out the PEO phase.

2.5. RGD surface modification

RGD modifications were carried out on the silk films as we have previously reported [44]. The silk films were presoaked in BupH^{TM} MES buffer (Pierce, Woburn, MA, 100 mM borate 150 mM and NaCl, pH 6.5) for 1 hour. The –COOH groups from the aspartic and glutamic acid residues in the silk fibroin were activated by reaction with 1-ethyl-3-(dimethylaminopropyl) carbodiimide hydrochloride (EDC_HCl)/N-hydroxysuccinimide (NHS) solution (0.5 mg/mL of EDC and 0.7 mg/mL of NHS in MES buffer, pH 6.5) for 45 min at room temperature to create the stable and amine-reactive NHS-esters on the silk film surface. The activated silk films were then washed with MES buffer three times and subsequently treated in 1 mg/mL GRGDS peptide (synthesized from Tufts University Core Facility) in MES buffer (pH 6.5) at room temperature for 3 hours. After GRGDS coupling reaction, the surface modified silk films were washed in MES buffer for two times and in ddH_2O for 5 times.

2.6. Transfected human cell culture

P7 immortalized human corneal keratocytes (hCFs) were kindly provided by May Griffith (Linköping University, Sweden). The human cell lines were isolated from donor cornea and immortalized by infection with an amphotropic recombinant retrovirus containing HPV16 genes E6 and E7 and with mammalian expression vectors containing genes encoding SV40 large T antigen, pSV3neo, and adenovirus E1A 12S, as described previously [3]. The cells were cultured in DMEM medium containing 10% FBS, 1% interferon–transferrin–selenium (ITS), and 1% PSF (Gibco, Pascagoula, MS). The cultures were harvested with 0.05% trypsin with 0.4 mM EDTA.

2.7. DNA content

hCF viability on silk substrates was evaluated using the Pico Green assay (Invitrogen, Inc., Grand Island, NY). hCFs were seeded on silk films at a density of 5,000/cm^2 and cultured over 1, 4, 7, and 14 days before measuring DNA content. For the Pico Green assay, samples were washed twice with PBS and subsequently incubated in 1 mL of 0.1% Triton-X 100 in 1 × TE buffer for 48 h. The sample supernatant was spun down by centrifugation for 5 min at 10,000 rpm. Subsequently, 25 μL of supernatant and 75 μL of 1 × TE buffer were placed into 96-well plates and 100 μL of a 1:200 dilution of QuantiT PicoGreen (Invitrogen, Inc., Grand Island, NY) reagent was added to each well and read using a fluorimeter with an excitation wavelength of 480 nm and an emission wavelength of 520 nm.

2.8. Cell alignment analysis

hCFs were seeded on the silk films at a density of 20,000 cells/cm^2 and phase contrast images examined on the 2nd day with a Leica/Leitz DM RBE Microscope (Leica, Mannheim, Germany) or Zeiss Axiovert 40 CFL Microscope (Carl Zeiss AG, Oberkochen, Germany). The orientation of hCFs was analyzed with ImagePro 6 software. The orientation angle was determined by calculating the angle difference between the longest direction within the cell borders and the silk film grooves. Over 2 days in culture, the angle difference between the longest axis of the cell boundary and the groove direction was measured from all existing cells shown in 10X phase contrast images. The mean orientation angles of hCFs grown on the flat,

patterned, and patterned/porous films with/without RGD surface modification was calculated from three individual 10X phase contrast images.

2.9. Real-Time-Reverse Transcription Polymerase Chain Reaction (Real Time RT-PCR)

hCFs were seeded at a density of 20,000 cells/cm^2 on the silk films. Over 7 and 14 day culture, total RNAs from each specimen (N=3 per group) were extracted using Trizo reagent (Invitrogen, Carlsbad, CA) and transferred into 2 ml plastic tubes. The tubes were centrifuged at 12,000 g for 10 min and the supernatant was transferred to a new tube. Chloroform (200 μL) was added to the solution and incubated for 5 min at room temperature. Tubes were again centrifuged at 12,000 g for 15 min and the upper aqueous phase was transferred to a new tube. One volume of 70% ethanol (v/v) was added and applied to an RNeasy mini spin column (Qiagen, Hilden, Germany). The RNA was washed and eluted according to the manufacturer's protocol. The RNA samples were reverse transcribed into cDNA using oligo (dT)-selection according to the manufacturer's protocol (High Capacity cDNA Archive Kit, Applied Biosystems, Foster City, CA). Collagen type I (Col I), collagen type V (Col V), decorin (DCR), and biglycan (BGN) gene expressions were quantified using the the M 3000 Real Time PCR system (Stratagene, CA). PCR reaction conditions were 2 min at 50°C, 10 min at 95°C, and then 50 cycles at 95°C for 15 s, and 1 min at 60°C. The expression data were normalized to the expression of the housekeeping gene, glyceraldehyde-3-phosphate-dehydrogenase (GAPDH). Probes for GAPDH, Col I, Col V, DCR, and BGN were purchased from Applied Biosciences (Foster City, CA).

2.10. Cytoskeleton and ECM alignment

hCFs were seeded at a density of 20,000 cells/cm^2 on the silk films and cultured for 6 days before taking images. Cell culture medium was gently removed and the silk films in culture plates were gently washed twice with PBS (pH 7.4). Subsequently, the samples were fixed for 10 min at room temperature using 4% paraformaldehyde solution. The 4% paraformaldehyde was removed with 3 subsequent PBS washings. Then the cells were permeabilized with PBS (pH 7.4) containing 0.2% Triton X-100 for 10 min, and blocked with PBS (pH 7.4) containing 1% BSA for 30 min. Actin filaments were stained using Texas Red-X phalloidan stain (Invitrogen, Inc., Grand Island, NY.), which was diluted using 10 μL of methanolic stock reagent and 400 μL of PBS for each sample. After diluting, 410 μL was placed onto each sample for 30 min with two subsequent PBS rinses. Primary antibodies for collagen type I (rabbit, Abcam, Inc., Cambridge, MA), collagen type V (mouse, Invitrogen, Inc., Grand Island, NY.), decorin (mouse, Abcam, Inc., Cambridge, MA), and byglycan (mouse, Abcam, Inc., Cambridge, MA) were diluted from their respective stock solutions to 5–10 μg/mL concentrations in PBS. 250 μL of antibody solution was placed onto each sample in 24 well plates and incubated at 4ºC for overnight. The samples were then washed 3 times with PBS and stained using Alexafluor 488 (anti-mouse, Invitrogen, Inc., Grand Island, NY) or Texas-red (anti-rabbit, Abcam, Inc., Cambridge, MA) as secondary antibody, in which a 10 μg/mL dilution was prepared. A 250 μL aliquot of secondary antibody solution was added to each sample for 30 min with 2 subsequent PBS rinses. Prolong anti-fading mounting media (Invitrogen, Inc., Grand Island, NY) was added on the samples and covered with cover glass. Confocal microscopy was carried out to examine cytoskeleton and ECM organization on the silk films. The middle z-section images of cells were taken by a Leica TCS SP2 AOBS confocal microscopy (Leica, Mannheim, Germany) equipped with 488 nm argon and 543 nm He/Ne lasers. Phalloidan staining excitation was at 543 nm and collected emission between 580 and 650 nm. Alexafluor 488 and Texas-red secondary antibody excitations were at 488 nm and 543 nm, respectively, and collected emission between 500 and 550 nm and between 580 and 650 nm, respectively. Confocal images of hCFs in the stacked 3D constructs (described below) were taken after 7 days in culture. 3D vertical projection images and z-sectional images with

cross sectional view were obtained by rendering 228 two-dimensional images with 400 nm interval within 91 μm depth.

2.11. 3D constructs of corneal stroma

Prepared RGD-coupled porous/patterned silk films (14 mm diameter) were sterilized in 70% ethanol for 30 min, air dried, washed 3 times in PBS (pH 7.4), and presoaked with hCF media overnight. The sterilized silk films were placed in tissue culture dish (10 cm diameter). PVC tube (12 mm inner diameter) was cut with around 7 mm height, autoclaved, and then the cut PVC rings were placed on each silk film to hold the films. Cells were then seeded upon the porous/patterned silk films at 100,000 cells/cm^2 seeding density and left to incubate for 48 h to allow for cell attachment. The seeded silk films were then carefully stacked one by one using applied pressure from a 12 mm biopsy punch; applying each pressure for each stacking. A total of 7 films were stacked per construct and the assembled construct were transferred into 6 well plates. The applied pressure was used to seal the stacked film construct together near the film edges, but did not pierce through the silk film substrate. Histological and confocal images of fixed and stained constructs were taken at day 7 after stacking.

2.12. Histological evaluation

After fixation with 4% phosphate-buffered formaldehyde for at least 24 h, specimens were embedded within paraffin and sectioned (10 μm). Using standard histochemical techniques, serial sections were stained with hematoxylin and eosin.

2.13. Statistical Methods

Results were statistically analyzed using one-way analysis of variance (ANOVA). A statistically significant difference was reported if $p<0.05$. Data are reported as the mean ± standard deviation (SD) with an N=3 or more.

3. Results

3.1. Preparation of silk films

Patterned silk film surfaces were cast from the patterned PDMS substrates prepared by casting on diffraction gratings as described in our previous reports [33,49]. Likewise, patterned/porous silk films were generated by casting a mixture of silk and PEO solution onto patterned PDMS molds, while flat silk film surfaces were obtained by casting silk solution onto flat PDMS surfaces. The as-cast films were water-annealed by incubation within a high humid vacuum environment to induce increased β-sheet formation that produces water insoluble films [29, 48]. The PEO aggregates in the silk films were leached out in water bath for 48 hours. Porous voids were left behind within the silk film matrix with pore size ranging between 500 nm and 10 μm in diameter and well distributed within the silk as observed previously [33] (data is not shown). The thickness of films was controlled to be 2 μm and we confirmed that pores (particularly, larger than 2 μm in diameter) extended through the film bulk. The combination of porous, patterned, and thin features in free-standing silk films allows for the construction of lamellae-like tissue scaffolds that can be assembled to produce a three-dimensional tissue construct. The prepared silk films were further modified by covalent coupling of RGD peptides to enhance cell attachment and proliferation.

3.2. hCFs Responses on silk substrates

The silk films were placed in 24 well plates, seeded with hCFs, and cultured *in vitro*. From the phase contrast images of hCFs on the silk surfaces over five days post-seeding, cell alignment was evident on both the patterned and patterned/porous silk surfaces (Figure 1c,e), while the hCFs were randomly oriented on flat silk surfaces (Figure 1a). However, hCFs were not

confluent on these silk films without RGD coupling over day 5 in culture (Figure 1a,c,e). In contrast, the silk surfaces with coupled RGD exhibited confluent cell coverage over 5 days in culture; flat silk films with RGD coupling showed confluent and randomly formed cell morphologies (Figure 1b), while patterned and patterned/porous silk films with RGD coupling showed confluent and aligned cell morphologies along with groove axis direction (Figure 1d,f). The magnified images show that hCFs grew over the pore structures (seen as white holes) within the silk film structures (2~10 μm in dia.). Cell bodies on the patterned and patterned/porous silk films appeared more elongated along the groove axis of the patterned surfaces compared to those on the flat films.

To quantify cell body alignment on the silk film surfaces, image analysis and subsequent statistical analysis was conducted from three 5X phase contrast images, after two days in culture (Figure 2). Mean cellular orientation angles were determined by calculating the angle difference between the longest direction within the cell borders and the grooves. hCFs cultured on the flat silk films showed a mean cellular orientation angle around 45º indicating that hCFs were randomly oriented, while hCFs cultured on the patterned films including patterned, patterned/porous, RGD-coupled patterned, and RGD-coupled patterned/porous films exhibited significantly reduced mean cellular orientation angles (11.1° ~ 13.5°) compared to the flat silk films. We observed no major shift of orientation angles with pores and RGD surface coupling; in contrast, we note that RGD modification on the patterned silk surface slightly increased hCF orientation. Thus, the ability of the surface pattern to align hCFs was not hindered by the combined pores and presence of RGD.

We next measured DNA content of hCFs grown on patterned, patterned/porous, and RGD coupled patterned/porous silk surfaces over a 14 day period to examine the effect of pores and RGD coupling on cell attachment and proliferation (Figure 3). DNA content increased with time for all films. Patterned/porous silk substrates exhibited slightly lower DNA contents of hCFs than the patterned silk substrates over 4 and 14 days in culture. In contrast, RGD coupled patterned/porous silk substrates exhibited significantly higher DNA content than the patterned/porous silk substrates on days 4, 7 and 14. Also, on day 1, RGD coupled patterned/porous silk substrates showed ~5% higher DNA content than the patterned/porous substrates even though the difference was not statistically significant. This indicates that RGD coupling enhanced hCF attachment and proliferation on silk surfaces, while the pores delayed hCF proliferation on silk surfaces.

3.3. Transcript expression of corneal stroma differentiation markers on silk substrates

Transcript expression of corneal stroma differentiation markers were quantified using real-time RT-PCR. Transcripts analyzed included collagen type I (Col I), collagen type V, decorin (DCR), and biglycan (BGN) (Figure 4). Transcript levels were normalized to GAPDH within the linear range of amplification and differences between silk film substrates were considered significant at $p<0.05$. After 7 days in culture, all transcription levels were not significantly different among flat, patterned/porous, and RGD-coupled patterned/porous silk films. After day 14 in culture, however, Col I, Col V, and DCR transcript levels increased in the patterned/porous constructs when compared with the flat silk substrates. Furthermore, RGD coupling on the patterned/porous silk substrates resulted in further increases of Col I, Col V, DCR, and BGN transcript levels when compared to both flat and patterned/porous silk substrates over 14 days of culture. We next compared differences in transcript levels of these markers between day 7 and day 14 in culture. Transcript levels of Col I, DCR, and BGN over day 14 in culture significantly increased in RGD-coupled patterned/porous silk films by 77%, 575% and 166%, respectively, while that of Col V increased by 29% without statistical significance, when compared with the values after 7 days in culture. In contrast, in the case of flat and patterned/porous silk films (silk films without RGD-coupling), transcript levels of Col I, Col V, and BGN

were significantly decreased or constant, while transcript levels of DCN were significantly increased by 122% and 346%, respectively. However, these increases were still lower than the increase in RGD-coupled patterned/porous silk films (575%).

3.4. Cytoskeleton alignment and extracellular matrix (ECM) orientation

After 6 days in culture, confocal images of hCF actin were obtained to investigate the cytoskeleton organization on the silk substrates. RGD-coupled patterned/porous silk films showed confluent actin filament alignment along with the patterned groove axis (Figure 5a), while flat silk films exhibited non-confluent and randomly formed actin filament deposition (Figure 5h). Higher magnification demonstrated cells interacting with the patterned and porous silk surface. These results agree with the apparent cell population and orientation on the RGD-coupled patterned/porous and flat silk film surfaces when hCFs were cultured over 6 days (Figure 1).

After 6 days in culture, immunocytochemistry confocal images were taken to examine expression and orientation of Col I, Col V (representative collagen types in human corneal stroma), DCR, and BGN (representative proteoglycans in human coreal stroma) on the silk substrates (Figure 5). Although high expression of these components was observed on all silk substrates, the features of the extracellular matrix deposition were different. Collagens and proteoglycans were randomly organized on the flat silk surfaces, while these components were aligned along with the groove axis on both patterned/porous and RGD-coupled patterned/porous silk films. This indicates that alignment of collagens and proteoglycans was governed by surface patterns regardless of RGD coupling. However, RGD-coupling affected deposition density of collagens and proteoglycans. Collagens and proteoglycans did not fully covered the entire surface of the flat and patterned/porous silk films. In contrast, these components were confluently covered on the RGD-coupled patterned/porous silk films. These results were coincident with the results of cell body orientation and population as seen in Figure 1. It is likely that collagens and proteoglycans were mainly organized around the cell bodies. The expression of collagens and proteoglycans suggests that the human corneal fibroblasts retained their differentiated phenotype on all the silk substrates and the organization of these components replicates the form of corneal stroma lamellae on both patterned/porous and RGD-coupled patterned/porous silk substrates.

3.5. Three-dimensional silk film tissue construct

RGD-coupled patterned/porous silk films were assembled to construct a three-dimensional lamellar scaffold to mimic the stromal layer of the cornea. The stacked silk films were prepared to include surface patterns, pores, and RGD coupling along with 2 μm film thickness (average stroma lamellae thickness). Before assembly, hCFs were seeded on the films and incubated for 48 h to allow for initial cell adhesion. Subsequently, seven cell seeded silk films were assembled. The assembly method was previously reported [33] but was modified; films were stacked one by one with applied pressure at each single film stacking step using a 12 mm biopsy bunch through hydrostatic bonding (Figure 6a) to obtain a corneal tissue equivalent assembly (Figure 6b). After an additional 7 days in culture, the corneal stroma equivalents were transparent as shown in Figure 6b, with a slight coloration due to media components.

Histological examination using hematoxylin and eosin was conducted to visualize the morphological features of the assembled silk film corneal tissue construct (Figure 6c). Corneal stroma tissue was well integrated with all layers in the construct. Some three dimensional growth of corneal stroma tissue was also observed (see arrow in Figure 6c) between the film layers. These histology images indicate that the assembled construct maintains cell proliferation and structural integrity after seven days in culture.

We next examined actin, collagen, and proteoglycan organization in the engineered corneal constructs. Immunostained 3D images of the assembled construct were obtained to visualized helicoidal alignment of corneal tissue matrix (Figure 7). Actin staining revealed hCF growth throughout the stacked construct with alignment along the groove direction; actin alignment was observed both near the silk film surface (Figure 7a) and over the silk film surface (Figure 7b). Pore structures within the silk film structure are seen as black holes in the silk film. Also, high expression and orientation of collagen type I and decorin (representative corneal stroma markers) along with the groove axis were obliquely observed in the 3D images through vertically projected images and z-sectional images of two middle layers with cross section (Figure 7c). ECMs aligned along with the groove axis of silk film layers, while each layer had a different alignment direction. Cross-sectional images (Figure7c-4~9) revealed spread cell morphologies similar to the in situ corneal keratocyte phenotype. These images show that the cells and native ECM in the assembled construct were viable and helicoidally aligned by replicating the structural hierarchy of the corneal stroma.

4. Discussion

A successful strategy for tissue engineering cornea should demonstrate proper biomaterial selection and optimized design to orchestrate cells and their production to replicate native tissue form and function. The present effort to construct human cornea tissue relied on the assembly of transparent and robust silk films functionalized with surface patterns and cell adhesion factors to guide helicoidal collagen fibril and native ECM alignment.

Silk biomaterials were bio-functionalized with RGD peptide and the tissue-engineered cornea formed that replicates native corneal stromal lamellar architecture with appropriate corneal stroma phenotypes and aligned collagen fibril lamellae after days 7 in culture. Initially, we hypothesized that RGD peptide decorations on silk protein films might anisotropically enhance interaction between basal surfaces of hCFs and patterned silk substrates, rather than non-patterned upper silk layers and apical surfaces of hCFs, due to polarity of integrins to improve function. Consequently, the RGD peptide decorations might help organize human corneal extracellular matrix (ECM) deposition and alignment specifically in a multi-lamellar construct.

Before addressing this hypothesis, we systematically studied the influence of RGD surface modification on cell alignment, attachment, proliferation, and differentiation. Our previous studies have shown that RGD peptide can be chemically coupled on silk films or sponge surfaces to increase osteoblast-like cell adhesion and expression of both alkaline phosphatase and osteocalcin [26,44,45]. The studies for hCF cell body alignment on the silk surfaces demonstrated that the surface modification with RGD did not hinder the ability of the topological cue of the silk surface grooves and slightly increased cell alignment on the patterned silk films. In contrast, DNA content of hCFs grown on these surfaces over culture time verified that the RGD surface coupling significantly enhanced cell attachment and proliferation on the patterned silk surfaces, while the pores in the films significantly reduced cell proliferation. Transcript expression of corneal stroma differentiation markers (Col I, Col V, DCR, and BGN) were also increased by RGD surface coupling as well as patterns on silk surface. Corneal fibroblasts can differentiate into a myofibroblast phenotype upon injury, where they do not highly express collagen type V during scar formation [50]. Also, decorin and biglycan are class I small leucine-rich proteoglycans (SLRPs) that play a role in the regulation of collagen fibril and matrix assembly in the extracellular matrix of connective tissue, including corneal stroma. Decorin is expressed in all developmental stages, while biglycan is highly expressed only at an early stage, decreasing during development, and present at very low levels in mature cornea [51].

The transcription expression of collagens and proteoglycans suggests that the human corneal fibroblasts retained their transcription genotype on the silk substrates and, also, that both patterned features and surfaces with RGD coupling up-regulated the expression of corneal stroma differentiation markers over 14 days in culture. We further studied actin and ECM expression and organization on the RGD coupled silk films from their immunostained confocal images. Col I, Col V, DCR, and BGN were highly expressed over the entire surface and were well aligned along the groove direction on the RGD-coupled patterned/porous silk films after days 6 in culture. These results demonstrated that the human corneal fibroblasts retained their differentiated phenotype and their ECM alignment while cultured on the RGD coupled silk films. Overall, RGD surface modification enhanced cell proliferation, alignment and expression of appropriate stroma phenotype markers. Thus, we realized that RGD-coupled patterned/porous silk films could be an appropriate option rather than just patterned/porous silk films to generate helicoidal alignment in 3D lamellar corneal constructs.

After systematic studies for hCFs response and ECM organization on the silk substrates, tissue-engineered human cornea silk biomaterials were constructed using the RGD-coupled patterned/porous silk films. The constructs composed of seven layers of silk films showed highly expressed and appropriate corneal stroma phenotype and angle-ply cytoskeleton and ECM laminates on the multi-layers along the groove directions after 7 days. The constructs also remained intact and transparent. These results elucidated that the cells and native ECM in the assembled construct were viable and aligned by replicating the structural hierarchy of the corneal stroma.

Although the corneal stroma tissue engineered in this study demonstrated the oriented multi-lamellar form and transparency to mimic native corneal stroma, many challenges remain before clinical implementation. In future studies optimization of the structural hierarchy to mimic the cornea will still be needed, including variables of: (i) orientation angle of layers with respect to each other, (ii) spacing between layers, (iii) degradation rate of the silk substrate during the formation of native ECM and (iv) number of stacked layers to be used. The average lamellar layer thickness in the human cornea is around 2 microns, and an overall cornea thickness is approximately 400 microns, consisting of around 200 collagen lamellae [6]. The 2 micron lamellar thickness is conserved within most vertebrates, including humans [6,52,53] and may relate to a balance between mechanical requirements, diffusion limitations, embedded stromal cell communication and fibril geometry. Thus, we need to determine how building up overall thickness impacts performance (mechanical, optical) as influenced by mass transfer through the layers. Furthermore, because the natural stroma has both the epithelium and endothelium to maintain fluid and ionic homeostasis [54], it is difficult to determine what diffusional limitations will be encountered for the layered constructs. In addition, we may need to employ several types of culture modifications instead of utilizing immortalized human corneal fibroblasts, since several corneal stromal cell phenotypes exist: keratocyte, fibroblast and myofibroblast. Finally, translation of these *in vitro* studies *in vivo* will require combinations with outer epithelium and inner endothelium and integration with the surrounding limbal tissues. Although further study should address these issues, this study successfully demonstrated significant progress in how to engineer *in vitro* helicoidal multi-lamellar tissue architectures that can replicate native corneal stroma form with alignment of cells and ECM anisotropy and its function with transparency and robustness. This strategy also has direct implications for other tissues due to the pervasive nature of such helicoidal structures in biological tissues.

5. Conclusions

We have demonstrated bio-functionalized silk protein-biomaterial lamellar systems coupled with human cornea fibroblasts for corneal tissue engineering. Silk biomaterials were

functionalized with RGD and the tissue-engineered cornea silk biomaterials were formed that replicate native corneal stromal lamellar architecture with appropriate corneal stromal phenotypes and aligned collagen fibril lamellae after day 7 in culture, while the constructs remained transparent. Furthermore, RGD surface modification enhanced cell attachment, proliferation, alignment and expression of corneal stroma markers, while surface pattern also increased expression of corneal stroma markers. The presented biomimetic approach to replicate corneal stromal tissue architecture demonstrates a useful strategy for engineering human cornea or numerous tissue needs.

Acknowledgments

The authors are grateful to May Griffith at the Linköping University for contributing the human corneal fibroblasts. This work was supported by the NIH R21 (EY01819) and the NIH P41 Tissue Engineering Resource Center (EB002520).

References

1. Morishige N, Petroll WM, Nishida T, Kenney MC, Jester JV. Noninvasive corneal stromal collagen imaging using two-photon-generated second-harmonic signals. J Cataract Refract Surg 2006;32(11): 1784–1791. [PubMed: 17081858]
2. Torbet J, Malbouyres M, Builles N, Justin V, Roulet M, Damour O, et al. Orthogonal scaffold of magnetically aligned collagen lamellae for corneal stroma reconstruction. Biomaterials 2007;28(29): 4268–4276. [PubMed: 17618680]
3. Griffith M, Osborne R, Munger R, Xiong XJ, Doillon CJ, Laycock NLC, et al. Functional human corneal equivalents constructed from cell lines. Science 1999;286(5447):2169–2172. [PubMed: 10591651]
4. Eye Bank Association of America. Annual report. 2005.
5. Mannis MJ, McDonough G, Howard K, Morales R, Sugar J. Screening donor corneas that have undergone PRK. Cornea 1997;16(6):683–685. [PubMed: 9395879]
6. Cintron C, Covington H, Kublin CL. Morphogenesis of Rabbit Corneal Stroma. Invest Ophthalmol Vis Sci 1983;24(5):543–556. [PubMed: 6841000]
7. Birk DE, Fitch JM, Babiarz JP, Doane KJ, Linsenmayer TF. Collagen Fibrillogenesis Invitro - Interaction of Type-I and Type-V Collagen Regulates Fibril Diameter. J Cell Sci 1990;95:649–657. [PubMed: 2384532]
8. Birk DE, Fitch JM, Babiarz JP, Linsenmayer TF. Collagen Type-I and Type-V Are Present in the Same Fibril in the Avian Corneal Stroma. J Cell Biol 1988;106(3):999–1008. [PubMed: 3346334]
9. Donohue DJ, Stoyanov BJ, Mccally RL, Farrell RA. Numerical Modeling of the Corneas Lamellar Structure and Birefringence Properties. J Opt Soc Am A Image Sci Vis 1995;12(7):1425–1438.
10. Duan X, Sheardown H. Dendrimer crosslinked collagen as a corneal tissue engineering scaffold: Mechanical properties and corneal epithelial cell interactions. Biomaterials 2006;27(26):4608–4617. [PubMed: 16713624]
11. Duan XD, McLaughlin C, Griffith M, Sheardown H. Biofunctionalization of collagen for improved biological response: Scaffolds for corneal tissue engineering. Biomaterials 2007;28(1):78–88. [PubMed: 16962168]
12. Crabb RAB, Chau EP, Evans MC, Barocas VH, Hubel A. Biomechanical and microstructural characteristics of a collagen film-based corneal stroma equivalent. Tissue Eng 2006;12(6):1565–1575. [PubMed: 16846352]
13. Hu XJ, Lui W, Cui L, Wang M, Cao YL. Tissue engineering of nearly transparent corneal stroma. Tissue Eng 2005;11(11–12):1710–1717. [PubMed: 16411816]
14. Myung D, Koh W, Bakri A, Zhang F, Marshall A, Ko JM, et al. Design and fabrication of an artificial cornea based on a photolithographically patterned hydrogel construct. Biomed Microdevices 2007;9 (6):911–922. [PubMed: 17237989]
15. Griffith M, Osborne R, Munger R, Xiong X, Doillon CJ, Laycock NL, et al. Functional human corneal equivalents constructed from cell lines. Science 1999;286(5447):2169–2172. [PubMed: 10591651]

16. Alaminos M, Del Carmen Sanchez-Quevedo M, Munoz-Avila JI, Serrano D, Medialdea S, Carreras I, et al. Construction of a complete rabbit cornea substitute using a fibrin-agarose scaffold. Invest Ophthalmol Vis Sci 2006;47(8):3311–3317. [PubMed: 16877396]
17. Lawrence BD, Marchant JK, Pindrus MA, Omenetto FG, Kaplan DL. Silk film biomaterials for cornea tissue engineering. Biomaterials 2009;30(7):1299–1308. [PubMed: 19059642]
18. Torbet J, Malbouyres M, Builles N, Justin V, Roulet M, Damour O, et al. Orthogonal scaffold of magnetically aligned collagen lamellae for corneal stroma reconstruction. Biomaterials 2007;28(29): 4268–4276. [PubMed: 17618680]
19. Hu X, Lui W, Cui L, Wang M, Cao Y. Tissue engineering of nearly transparent corneal stroma. Tissue Eng 2005;11(11–12):1710–1717. [PubMed: 16411816]
20. Mimura T, Amano S, Yokoo S, Uchida S, Yamagami S, Usui T, et al. Tissue engineering of corneal stroma with rabbit fibroblast precursors and gelatin hydrogels. Mol Vis 2008;14:1819–1828. [PubMed: 18852871]
21. Crabb RA, Chau EP, Evans MC, Barocas VH, Hubel A. Biomechanical and microstructural characteristics of a collagen film-based corneal stroma equivalent. Tissue Eng 2006;12(6):1565–1575. [PubMed: 16846352]
22. Nishida K, Yamato M, Hayashida Y, Watanabe K, Yamamoto K, Adachi E, et al. Corneal reconstruction with tissue-engineered cell sheets composed of autologous oral mucosal epithelium. N Engl J Med 2004;351(12):1187–1196. [PubMed: 15371576]
23. Liu W, Merrett K, Griffith M, Fagerholm P, Dravida S, Heyne B, et al. Recombinant human collagen for tissue engineered corneal substitutes. Biomaterials 2008;29(9):1147–1158. [PubMed: 18076983]
24. Rafat M, Li F, Fagerholm P, Lagali NS, Watsky MA, Munger R, et al. PEG-stabilized carbodiimide crosslinked collagen-chitosan hydrogels for corneal tissue engineering. Biomaterials 2008;29(29): 3960–3972. [PubMed: 18639928]
25. Panilaitis B, Altman GH, Chen JS, Jin HJ, Karageorgiou V, Kaplan DL. Macrophage responses to silk. Biomaterials 2003;24(18):3079–3085. [PubMed: 12895580]
26. Meinel L, Hofmann S, Karageorgiou V, Kirker-Head C, McCool J, Gronowicz G, et al. The inflammatory responses to silk films in vitro and in vivo. Biomaterials 2005;26(2):147–155. [PubMed: 15207461]
27. Shao ZZ, Vollrath F. Materials: Surprising strength of silkworm silk. Nature 2002;418(6899):741–741. [PubMed: 12181556]
28. Motta A, Fambri L, Migliaresi C. Regenerated silk fibroin films: Thermal and dynamic mechanical analysis. Macromol Chem Physic 2002;203(10–11):1658–1665.
29. Jin HJ, Park J, Karageorgiou V, Kim UJ, Valluzzi R, Kaplan DL. Water-stable silk films with reduced beta-sheet content. Advanced Functional Materials 2005;15(8):1241–1247.
30. Wang Y, Rudym DD, Walsh A, Abrahamsen L, Kim HJ, Kim HS, et al. In vivo degradation of three-dimensional silk fibroin scaffolds. Biomaterials 2008;29(24–25):3415–3428. [PubMed: 18502501]
31. Servoli E, Maniglio D, Motta A, Predazzer R, Migliaresi C. Surface properties of silk fibroin films and their interaction with fibroblasts. Macromol Biosci 2005;5(12):1175–1183. [PubMed: 16315185]
32. Sugihara A, Sugiura K, Morita H, Ninagawa T, Tubouchi K, Tobe R, et al. Promotive effects of a silk film on epidermal recovery from full-thickness skin wounds. Proc Soc Exp Biol Med 2000;225 (1):58–64. [PubMed: 10998199]
33. Lawrence BD, Marchant JK, Pindrus MA, Omenetto FG, Kaplan DL. Silk film biomaterials for cornea tissue engineering. Biomaterials 2009;30(7):1299–1308. [PubMed: 19059642]
34. Gil ES, Park SH, Marchant J, Omenetto F, Kaplan DL. Response of Human Corneal Fibroblasts on Silk Film Surface Patterns. Macromol Biosci 2010;10(6):664–673. [PubMed: 20301120]
35. Gupta MK, Khokhar SK, Phillips DM, Sowards LA, Drummy LF, Kadakia MP, et al. Patterned silk films cast from ionic liquid solubilized fibroin as scaffolds for cell growth. Langmuir 2007;23(3): 1315–1319. [PubMed: 17241052]
36. Perry H, Gopinath A, Kaplan DL, Dal Negro L, Omenetto FG. Nano- and micropatterning of optically transparent, mechanically robust, biocompatible silk fibroin films. Adv Mater 2008;20(16):3070–3072.
37. Omenetto FG, Kaplan DL. A new route for silk. Nat Photonics 2008;2(11):641–643.

38. Boateng SY, Lateef SS, Mosley W, Hartman TJ, Hanley L, Russell B. RGD and YIGSR synthetic peptides facilitate cellular adhesion identical to that of laminin and fibronectin but alter the physiology of neonatal cardiac myocytes. Am J Physiol Cell Physiol 2005;288(1):C30–C38. [PubMed: 15371257]
39. Jung HJ, Ahn KD, Han DK, Ahn DJ. Surface characteristics and fibroblast adhesion behavior off RGD-immobilized biodegradable PLLA films. Macromol Res 2005;13(5):446–452.
40. Yang XB, Roach HI, Clarke NMP, Howdle SM, Quirk R, Shakesheff KM, et al. Human osteoprogenitor growth and differentiation on synthetic biodegradable structures after surface modification. Bone 2001;29(6):523–531. [PubMed: 11728922]
41. Yoon JJ, Song SH, Lee DS, Park TG. Immobilization of cell adhesive RGD peptide onto the surface of highly porous biodegradable polymer scaffolds fabricated by a gas foaming/salt leaching method. Biomaterials 2004;25(25):5613–5620. [PubMed: 15159077]
42. Jun HW, West J. Development of a YIGSR-peptide-modified polyurethaneurea to enhance endothelialization. J Biomater Sci Polym Ed 2004;15(1):73–94. [PubMed: 15027844]
43. Doane KJ, Yang G, Birk DE. Corneal Cell Matrix Interactions - Type-Vi Collagen Promotes Adhesion and Spreading of Corneal Fibroblasts. Exp Cell Res 1992;200(2):490–499. [PubMed: 1572410]
44. Sofia S, McCarthy MB, Gronowicz G, Kaplan DL. Functionalized silk-based biomaterials for bone formation. J Biomed Mater Res 2001;54(1):139–148. [PubMed: 11077413]
45. Chen JS, Altman GH, Karageorgiou V, Horan R, Collette A, Volloch V, et al. Human bone marrow stromal cell and ligament fibroblast responses on RGD-modified silk fibers. J Biomed Mater Res A 2003;67A(2):559–570. [PubMed: 14566798]
46. Gil ES, Park SH, Marchant J, Omenetto F, Kaplan DL. Response of Human Corneal Fibroblasts on Silk Film Surface Patterns. Macromol Biosci 2010;10(6):664–673. [PubMed: 20301120]
47. Kim UJ, Park J, Kim HJ, Wada M, Kaplan DL. Three-dimensional aqueous-derived biomaterial scaffolds from silk fibroin. Biomaterials 2005;26(15):2775–2785. [PubMed: 15585282]
48. Lawrence BD, Omenetto F, Chui K, Kaplan DL. Processing methods to control silk fibroin film biomaterial features. J Mater Sci 2008;43(21):6967–6985.
49. Lawrence BD, Cronin-Golomb M, Georgakoudi I, Kaplan DL, Omenetto FG. Bioactive silk protein biomaterial systems for optical devices. Biomacromolecules 2008;9(4):1214–1220. [PubMed: 18370418]
50. Tomasek JJ, Gabbiani G, Hinz B, Chaponnier C, Brown RA. Myofibroblasts and mechano-regulation of connective tissue remodelling. Nat Rev Mol Cell Bio 2002;3(5):349–363. [PubMed: 11988769]
51. Zhang G, Chen S, Goldoni S, Calder BW, Simpson HC, Owens RT, et al. Genetic Evidence for the Coordinated Regulation of Collagen Fibrillogenesis in the Cornea by Decorin and Biglycan. J Biol Chem 2009;284(13):8879–8888.
52. Hogan, MJ.; Alvarado, JA.; Weddell, JE. Histology of the Human Eye. Philadelphia: W.B. Saunders; 1971.
53. Steele C. Corneal wound healing: a review. Optom Today 1999;9:28–32.
54. Ethier CR, Johnson M, Ruberti J. Ocular biomechanics and biotransport. Annu Rev Biomed Eng 2004;6:249–273. [PubMed: 15255770]

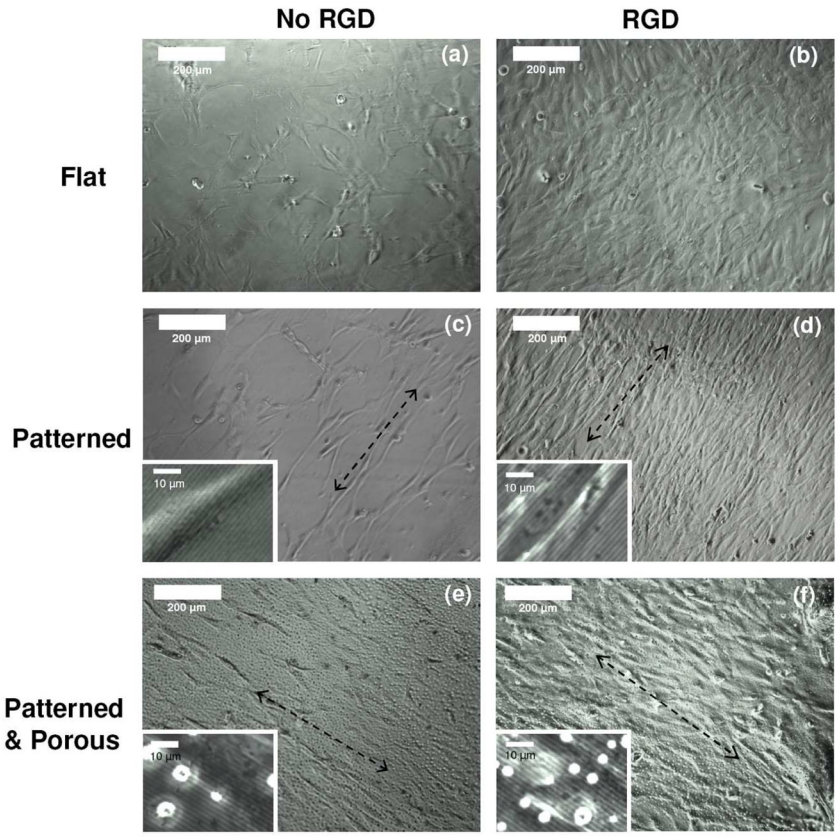

Figure 1.

Phase contrast optical micrographs of hCFs grown on silk films without (a, c, e) and with (b, d, f) RGD surface modification over 5 days in culture: flat (a, b), patterned (c, d) and patterned/porous (e, f). The magnified images reveal that hCFs are aligned on the patterned silk surface along with the groove axis and that hCFs are grown over pore structures (seen as white holes) within the silk film structure (2 ~ 10 μm in dia.).

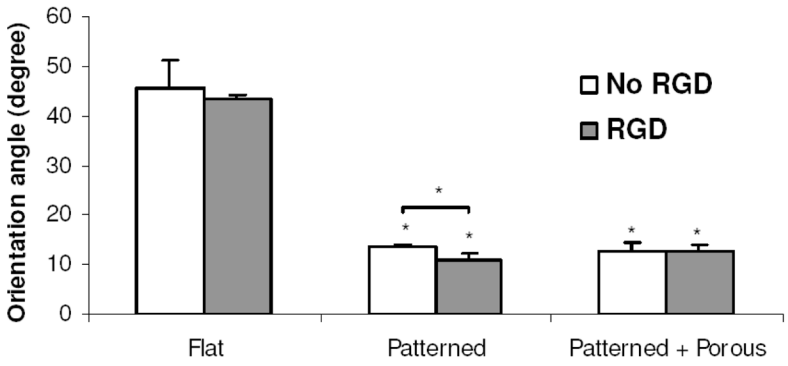

Figure 2.

Mean orientation angles of hCFs grown on the flat and patterned silk films. The orientation angle was determined by calculating the angle difference between the longest direction within the cell borders and the grooves. The mean orientation angle was defined by the mean±SD of three orientation angles averaged from three individual 10X images. (N=3, Cell population in each image varied from 25 to 58. Bars represent SD)

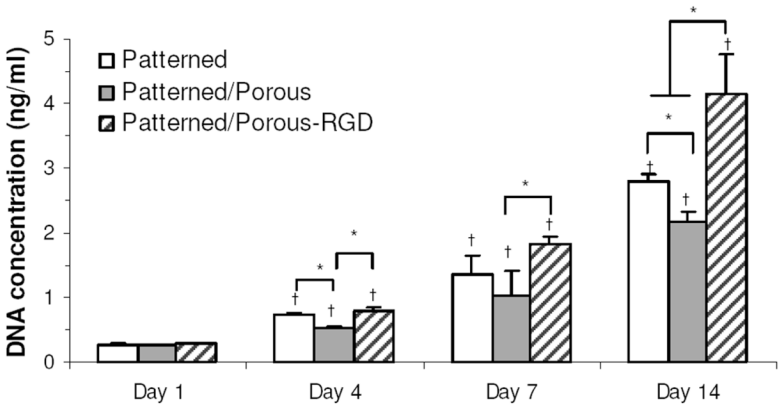

Figure 3.

DNA content for hCFs grown on patterned, patterned/porous, and RGD coupled patterned/porous silk film substrates after 1~7 days in culture ($p<0.05$, N=4. Bars represent SD).

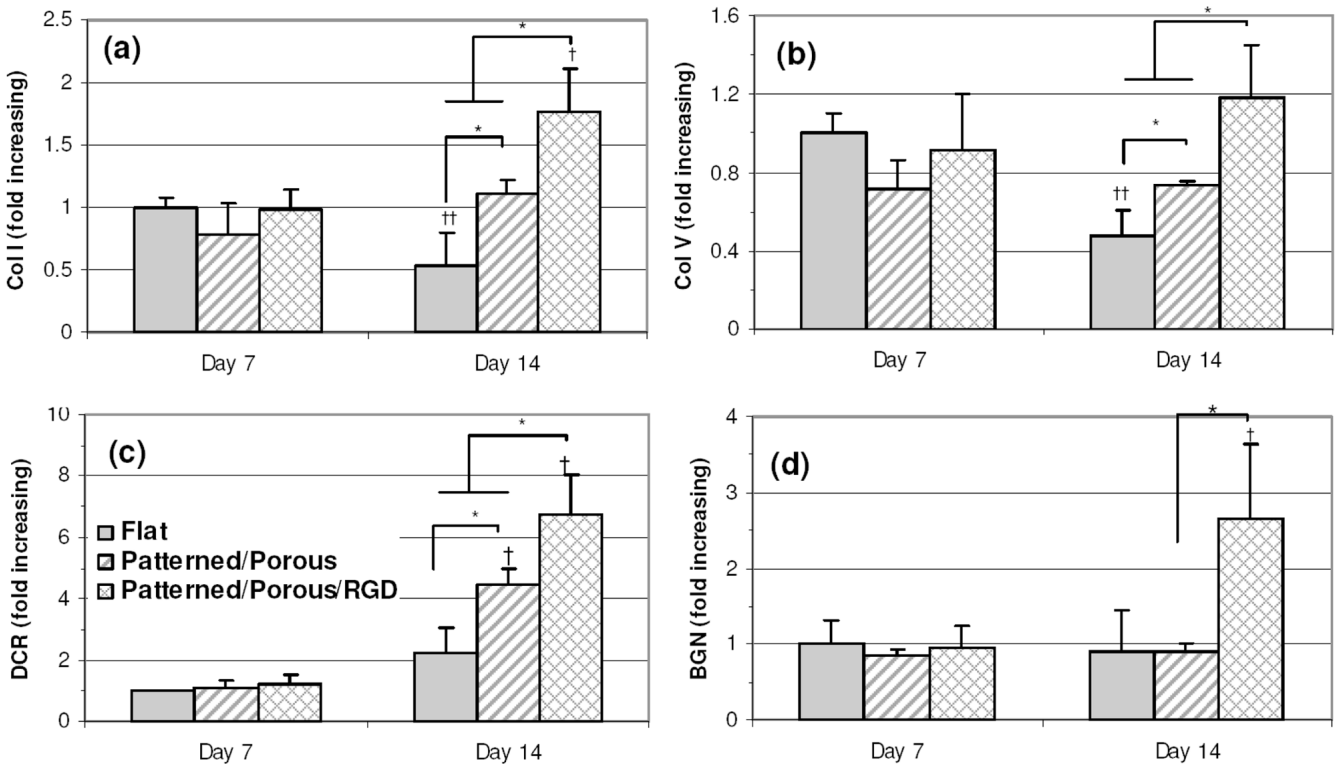

Figure 4.

Expression of transcripts related to corneal stroma differentiation. Transcript expression of corneal stroma differentiation markers quantified by real-time RT-PCR; (a) Collagen Type I (Col I), (b) Collagen Type V (Col V), (c) Decorin (DCR), (d) Biglycan (BGN). Transcript levels were normalized to GAPDH within the linear range of amplification. *represents statistical significance between means of different substrate groups at similar time points; † and †† indicate statistical significance (increase and decrease, respectively) between means of similar substrate groups at different time points ($p<0.05$, N=3. Bars represent SD)

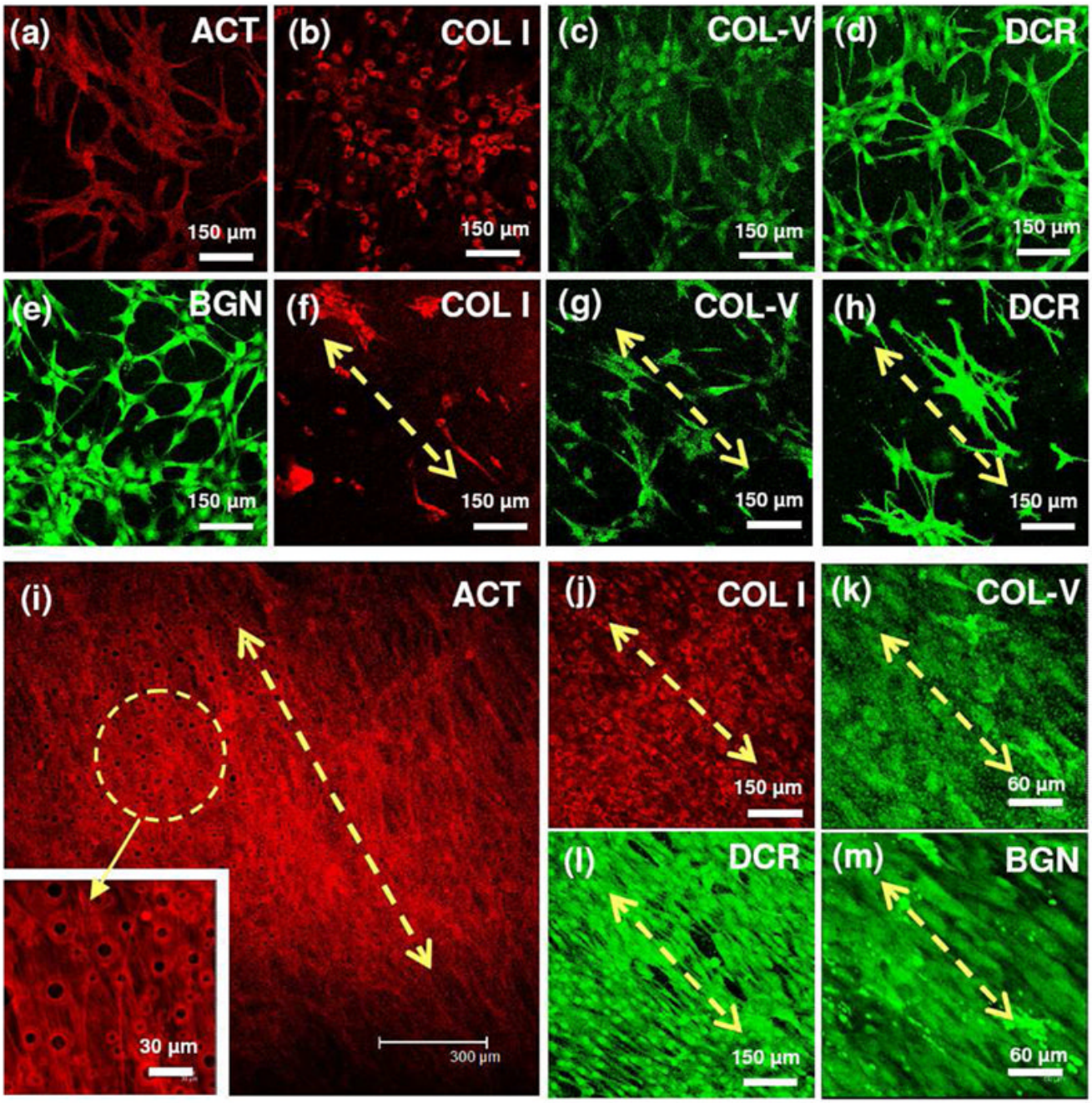

Figure 5.
Confocal images of hCFs after 6 days in culture on flat (a–e), patterned/porous (f–h), and RGD-coupled patterned/porous silk films (i–m); actin filaments (ACT) (a, i) and immunostained collagen type I (Col I) (a, f, j), immunostained collagen type V (Col V) (c, g, k), immunostained decorin (DCR) (d, h, l), immunostained biglycan (BGN) (e, m).

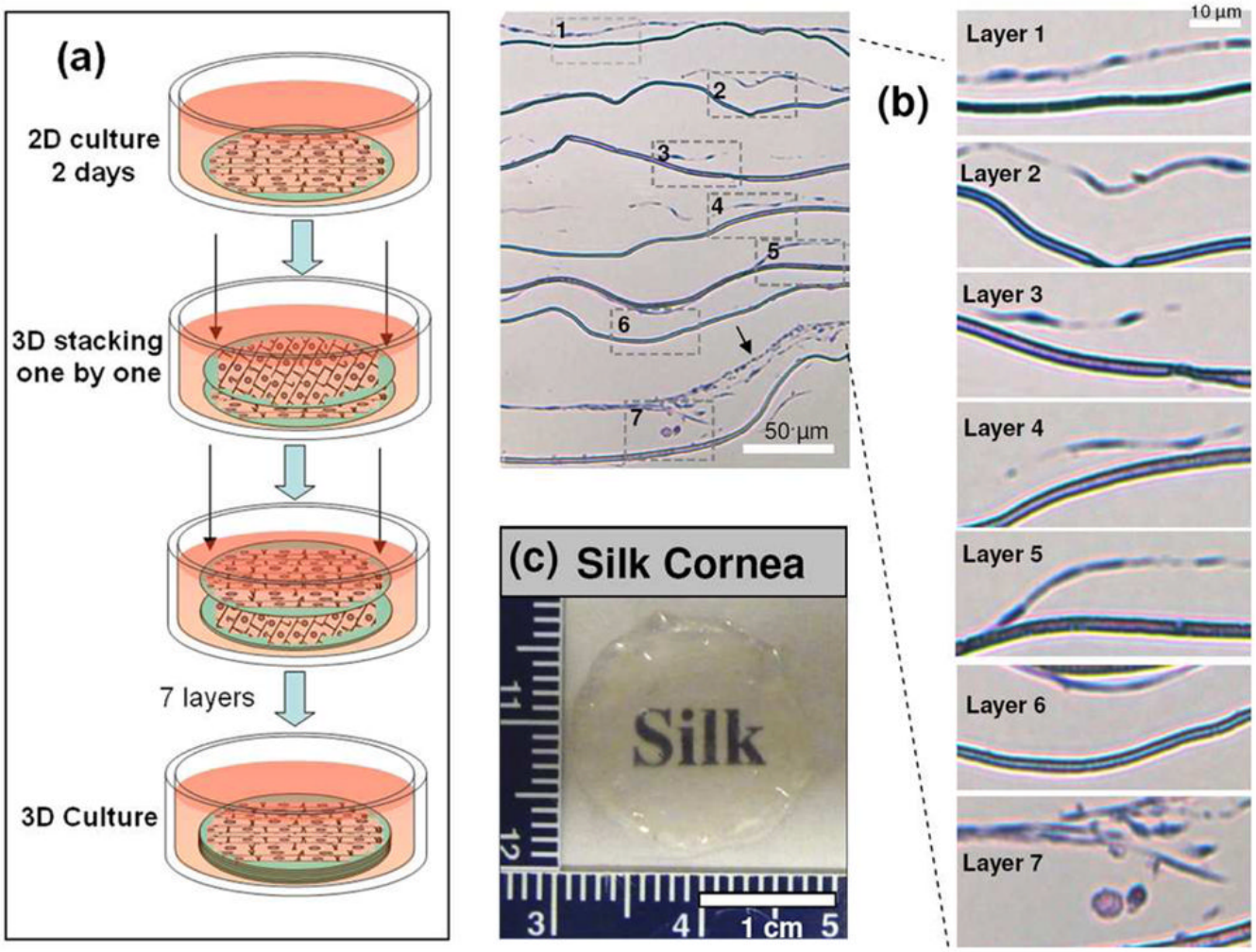

Figure 6.

(a) Schematic of the assembly process for three-dimensional (3D) silk film corneal constructs. PVC rings (12 mm diameter) were placed on each silk film to hold the films before cell seeding at 100,000 cells/cm^2 seeding density. After 2 days, hCFs layers with silk films were stacked one by one with applied pressure at each single film stacking step by using a 12 mm biopsy bunch and then the stacked constructs were cultured for 1 wk. Patterned and porous silk films with RGD surface modification were utilized for 3D corneal constructs. (b) Hematoxylin and eosin staining of cells on silk constructs after cultured for 1 wk. Arrow indicates three dimensional growth of corneal stroma tissue between the film layers. (c) Photo of stacked constructs after 1 wk. The constructs were visually clear enough to see the letters below.

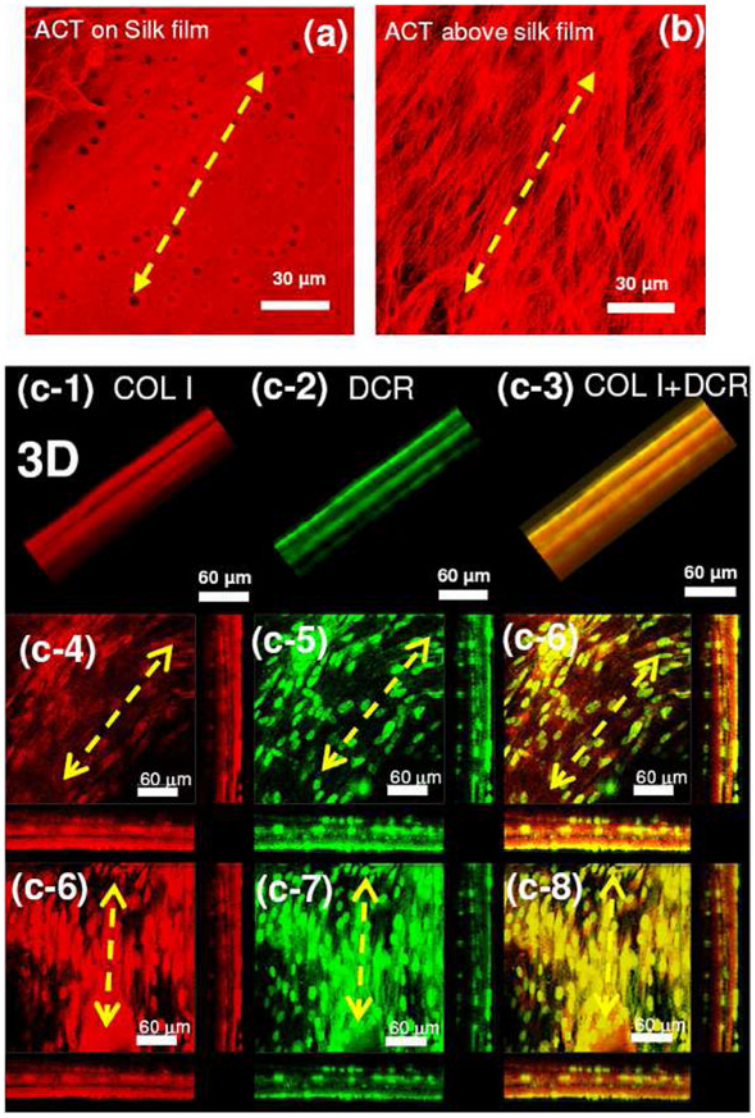

Figure 7.

Confocal images of hCFs in stacked 3D constructs after 7 d. Confocal images of stained actin filament near the silk film (a) and over the silk film (b) (both were obtained from same X-Y position) in the 3D constructs. 3D images (vertically projected images (c-1,2,3) and z-sectional images of two middle layers with cross section (c-4~8)). Red = immunostained collagen I (c-1,4,6), Green = immunostained decorin (c-2,5,7), and overlay images of decorin and collagen I (c-3,6,8).